Electrochemical and Solid-State Letters, **9** (3) A105-A109 (2006)
1099-0062/2006/9(3)/A105/5/$20.00 © The Electrochemical Society

A Proton-Conducting In^{3+}-Doped SnP_2O_7 Electrolyte for Intermediate-Temperature Fuel Cells

Masahiro Nagao,[a,*] Akihiko Takeuchi,[a] Pilwon Heo,[a] Takashi Hibino,[a,,z] Mitsuru Sano,[a] and Atsuko Tomita[b]**

[a]*Graduate School of Environmental Studies, Nagoya University, Nagoya 464-8601, Japan*
[b]*National Institute of Advanced Industrial Science and Technology, Nagoya 463-8560, Japan*

We report proton conduction in In^{3+}-doped SnP_2O_7 in the temperature range from 100 to 300°C, and the performance of a H_2-air fuel cell using this material as the electrolyte. The proton conductivity of In^{3+}-doped SnP_2O_7 was more than 10^{-1} S cm^{-1} between 125 and 300°C, and a conductivity value of 1.95×10^{-1} S cm^{-1} was achieved at 250°C. The resulting fuel cell exhibited a reasonable power density of 264 mW cm^{-2} at 250°C (electrolyte thickness = 0.35 mm), together with perfect tolerance toward 10% CO and good thermal stability in unhumidified conditions.
© 2006 The Electrochemical Society. [DOI: 10.1149/1.2159298] All rights reserved.

Manuscript submitted July 25, 2005; revised manuscript received September 14, 2005. Available electronically January 12, 2006.

Considerable effort has recently been devoted toward the development of solid-state proton conductors with conductivities $>10^{-2}$ S cm^{-1} in the temperature range of 150 to 400°C. Although a number of hydrous proton conductors have been reported thus far, most of them cannot meet these criteria. This is because protons attach themselves to water and diffuse as H_3O^+ ions through the solid (vehicular mechanism),[1] which limits the operating temperature to the dehydration temperature of ~100°C. On the other hand, anhydrous proton conductors can, in principle, avoid this problem since in these materials, protons migrate via jumps between adjacent oxide ions by a series of making and breaking of hydrogen bonds (Grotthuss mechanism).[1] Such proton conductors usually consist of oxyanions (SO_4^{2-} or PO_4^{3-}), wherein an oxide ion is joined to a proton by a hydrogen bond. However, there is a temperature limitation on the use of sulfonate-based proton conductors due to thermal decomposition of the SO_4^{2-} ions above 200°C.[2] Therefore, attention has recently been increasingly focused on phosphate-based proton conductors which are stable up to 200°C or higher. Various types of phosphate-based proton conductors have been investigated thus far, including inorganic crystals,[3-5] glasses (or gels),[6,7] and inorganic/organic composites.[8,9] In particular, CsH_2PO_4 is a very promising material as an intermediate-temperature proton conductor showing a conductivity of 2.0×10^{-2} S cm^{-1} at a temperature of 235°C and a water partial pressure (p_{H_2O}) of 0.3 atm.[5] A further increase in proton conductivities and a further reduction in the relative humidity would enhance the position of intermediate-temperature fuel cells as the preferred electric power generation devices.

In our previous study, we found that an anhydrous proton conductor, SnP_2O_7, showed high proton conductivities $>10^{-2}$ S cm^{-1} between 150 and 300°C under unhumidified conditions.[10] This material has a cubic or pseudo-cubic structure over a wide temperature range, characterized by SnO_6 octahedra at the corners and P_2O_7 units at the edges.[11] There are nominally no structural protons in SnP_2O_7, suggesting that protons dissolve as defects in the presence of hydrogen-containing gases. A similar proton incorporation mechanism has been proposed for Ca^{2+}- or Sr^{2+}-doped $LaPO_4$ in phosphate-based proton conductors.[12,13] However, the proton conductivities of the $LaPO_4$-based proton conductors were much lower than those of SnP_2O_7 in the temperature range from 150 to 300°C, probably due to the difference in their constituent oxyanions ($P_2O_7^{4-}$ and PO_4^{3-}). Indeed, our previous study showed that the conductivity of $SnHPO_4$ was about three orders of magnitude lower than that of SnP_2O_7.[10]

The primary goal of this study was to improve the proton conductivity of SnP_2O_7 by the substitution of In^{3+} cations for a portion of Sn^{4+} cations, and to investigate proton conduction using various techniques. We also attempted to demonstrate the feasibility of operating an intermediate-temperature fuel cell using this material. In particular, our interest is centered on fuel-cell performance under unhumidified conditions and on the tolerance of the platinum electrocatalyst to CO.

Experimental

In^{3+}-doped SnP_2O_7 was prepared as follows. SnO_2 and In_2O_3 powders were mixed with 85% H_3PO_4 and held with stirring at 300°C until the mixture formed a paste with a high viscosity. The pastes thus prepared were calcined in an alumina pot at 650°C for 2.5 h and then ground into powder with a mortar and pestle. The final P/(Sn + In) molar ratio of the compounds was confirmed to be 2.0 (±0.02) from X-ray fluorescence (XRF) measurements. The crystalline structure of the compounds was analyzed by X-ray diffraction (XRD). Fourier transform infrared (FTIR) spectra of the compounds were measured in the transmission mode by the KBr pellets technique, and data points were obtained in 60 scans with a resolution of 4 cm^{-1}. Temperature programmed desorption (TPD) spectra of the compounds were measured on a conventional TPD apparatus with an on-line mass spectrometer. The sample powders were heated in a stream of humidified argon at 200°C for 2 h. After purging with dry argon (99.999%) for 12 h, the sample powders were heated at a rate of 5°C min^{-1} until the evolution of gases was completed.

For impedance spectra and galvanic cell measurements, the compound powders were pressed into pellets under a pressure of 2×10^3 kg cm^{-2}. Impedance spectra measurements were carried out by the standard four-probe method. The frequency range was 0.1–10^6 Hz, and the ac amplitude was 10 mV. The H/D isotope effect on conductivity was also investigated by replacing argon with p_{H_2O} = 0.03 atm with argon with p_{D_2O} = 0.03 atm. Three types of galvanic cells, H_2, and steam concentration cells, and a H_2/air fuel cell, were fabricated using the pellets (thickness: 0.35 or 1.2 mm, diameter: 12 mm) as the electrolyte membrane. Both the anode and cathode (area: 0.5 cm^2) were made from a catalyst (10 wt % Pt/C, E-TEK) and carbon paper (Toray TGPH-090), wherein the Pt loading was 0.6 mg cm^{-2}. An intermediate layer, prepared by mixing 60 wt % of 10 wt % Pt/C and 40 wt % of 10 mol % In^{3+}-doped SnP_2O_7, was brushed on the electrode as uniformly and thinly as possible. The separation of the ohmic and polarization resistances was performed by a current interruption method. In this case, a Pt reference electrode was attached to the surface on the side of the electrolyte membrane.

Results and Discussion

Figure 1 shows typical XRD patterns for undoped and In^{3+}-doped SnP_2O_7 measured at room temperature. The peaks ob-

* Electrochemical Society Student Member.
** Electrochemical Society Active Member.
z E-mail: hibino@urban.env.nagoya-u.ac.jp

Downloaded on 2013-08-25 to IP 133.6.32.9 address. Redistribution subject to ECS license or copyright; see ecsdl.org/site/terms_use

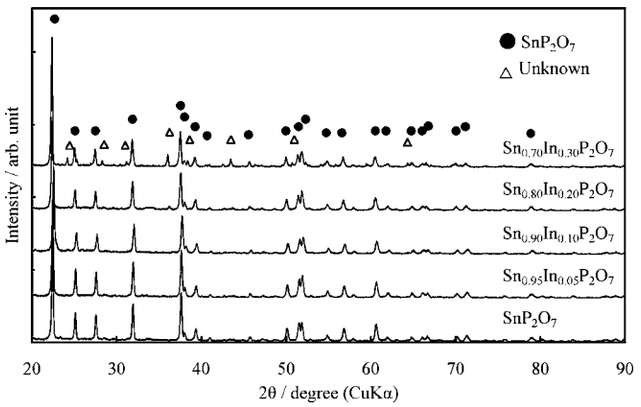

Figure 1. XRD patterns of undoped and In^{3+}-doped SnP_2O_7.

served for SnP_2O_7 were almost identical to those reported in the literature.[11] SnP_2O_7 doped with In^{3+} content of not more than 10 mol % showed similar patterns to that of undoped SnP_2O_7, while SnP_2O_7 doped with In^{3+} contents of 20 and 30 mol % contained some other unidentified signals. These results suggest that an In^{3+} content of 10 mol % is a substitutable limit of In^{3+} for Sn^{4+}.

The conductivities of undoped and In^{3+}-doped SnP_2O_7 at different temperatures in unhumidified air (P_{H_2O} = ~0.0075 atm) are shown in Fig. 2. The substitution of In^{3+} for Sn^{4+} clearly enhanced conductivity, and an impurity phase formed for an In^{3+} content of more than 10 mol % deteriorated the conductivity. It should be noted that the conductivities of undoped and In^{3+}-doped SnP_2O_7 increased monotonously with increasing temperature, which is different from superprotonic behavior[1,2,5] that shows a sharp increase in the conductivity of a few orders of magnitude by a structural transition from a low- to a high-temperature phase. This is because SnP_2O_7 shows no structural transitions in the temperature range of

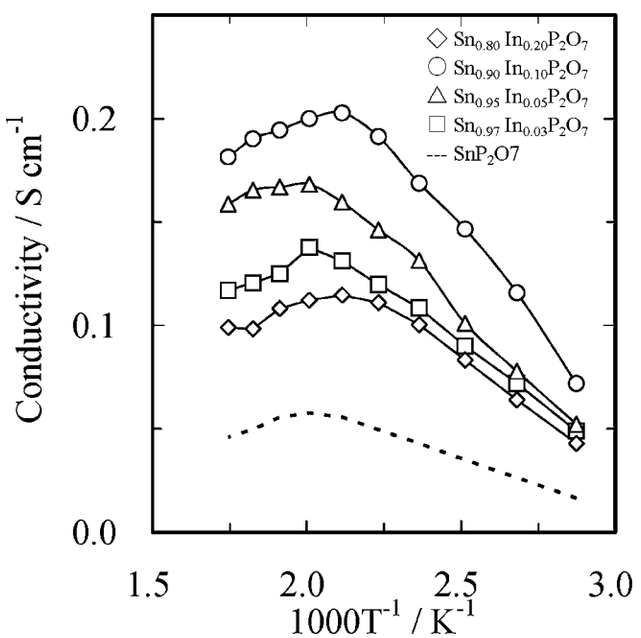

Figure 2. Temperature dependence of conductivity of undoped and In^{3+}-doped SnP_2O_7. The samples were maintained in unhumidified air (p_{H_2O} = ~0.0075 atm).

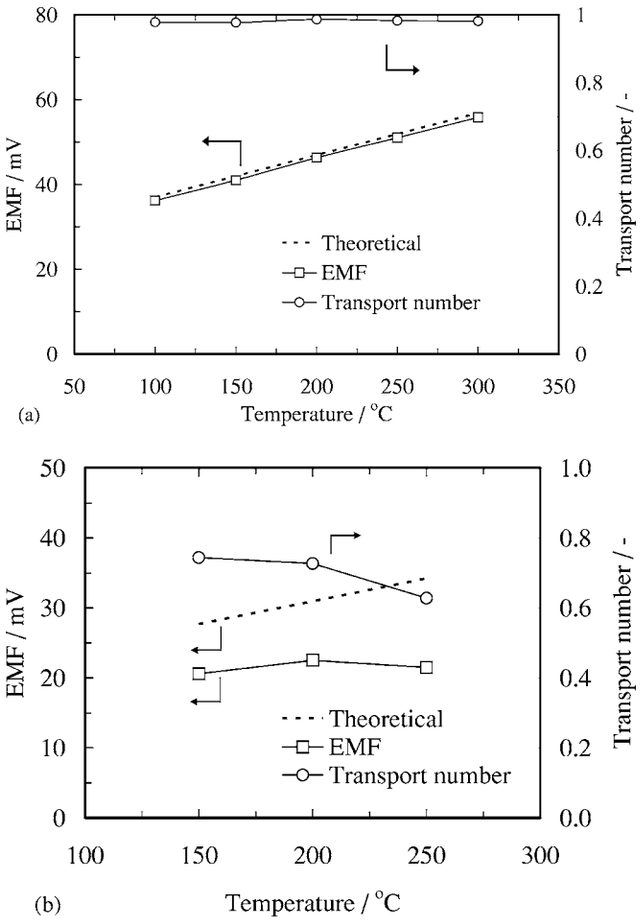

Figure 3. EMF values of various galvanic cells using $Sn_{0.9}In_{0.1}P_2O_7$ as an electrolyte membrane. (a) Anode gas = H_2 (1 atm); cathode gas = H_2 + Ar (0.1 atm). (b) Anode gas = air (p_{H_2O} = 0.031 atm); cathode gas = air (p_{H_2O} = 0.006 atm).

interest, as described above. In^{3+}-doped SnP_2O_7 ($Sn_{0.9}In_{0.1}P_2O_7$), 10 mol %, with the highest conductivity of 1.95×10^{-1} S cm^{-1} at 250°C was used in subsequent experiments.

A comparison of the electromotive force (EMF) value of the following galvanic cells with the theoretical value calculated from Nernst's equation was performed to understand the nature of the point defects in $Sn_{0.9}In_{0.1}P_2O_7$ under various conditions

$$H_2(1\ \text{atm}), Pt/C|Sn_{0.9}In_{0.1}P_2O_7|Pt/C, H_2 + Ar(0.1\ \text{atm}) \quad [1]$$

$$\text{air}(P_{H_2O} = 0.031), Pt/C|Sn_{0.9}In_{0.1}P_2O_7|Pt/C, \text{air}(P_{H_2O} = 0.006) \quad [2]$$

It can be seen from Fig. 3a that the EMF values observed for cell 1 were very near the theoretical values. We note that cell 1 is a H_2 concentration cell and also a sort of O_2 concentration cell, since the following equilibrium is established between O_2, H_2, and H_2O at each electrode

$$H_2 + \frac{1}{2}O_2 \leftrightarrows H_2O \quad [3]$$

Thus, the ratio of the EMF value to the theoretical value shows the ionic (proton or oxide ion) transport number, which was calculated to be about 0.98 at all temperatures. Details of mixed proton and O^{2-} ion conduction in the H_2 concentration cell have been reported by some research groups.[14-16] On the other hand, it is found in Fig.

Downloaded on 2013-08-25 to IP 133.6.32.9 address. Redistribution subject to ECS license or copyright; see ecsdl.org/site/terms_use

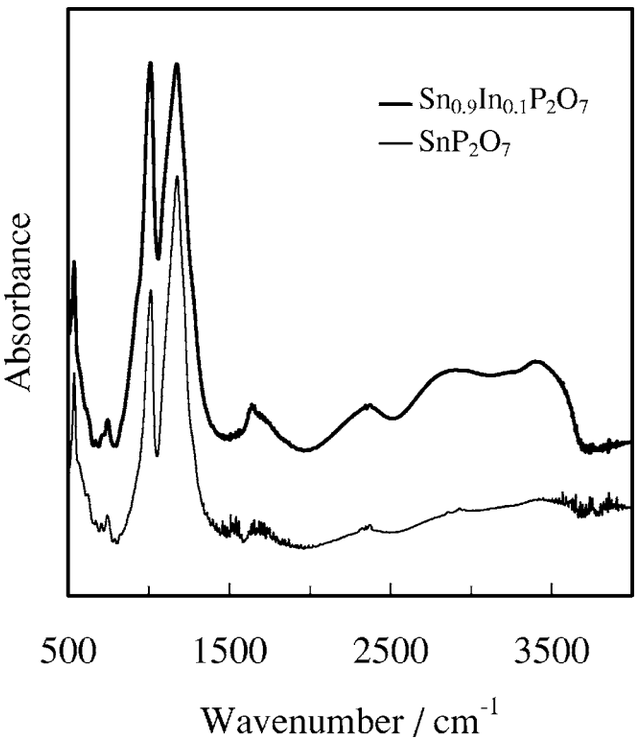

Figure 4. IR spectra for $Sn_{0.9}In_{0.1}P_2O_7$ and SnP_2O_7.

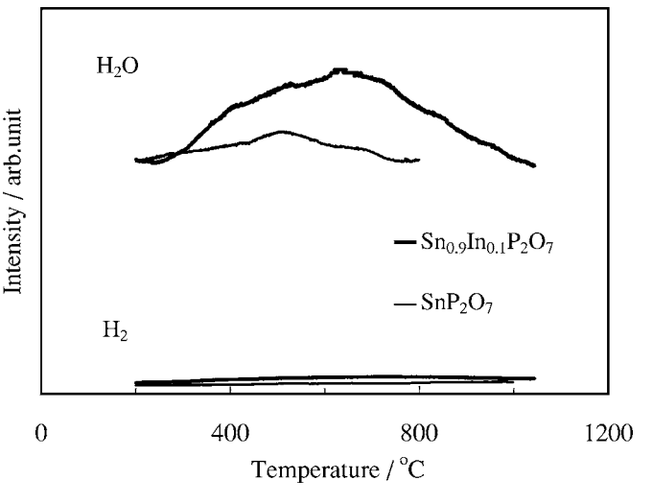

Figure 5. TPD spectra for $Sn_{0.9}In_{0.1}P_2O_7$ and SnP_2O_7.

3b that the EMF values observed for cell 2 were lower than the theoretical values. Although Eq. 3 is also applicable to cell 2, the difference in P_{O_2} between the electrodes caused by the difference in P_{H_2O} between them is negligibly small in the presence of excess O_2 (P_{O_2} = 0.21 atm). Therefore, the observed EMF is attributable to proton conduction in $Sn_{0.9}In_{0.1}P_2O_7$, meaning that the proton transport number is in the range from 0.63 to 0.74 in humidified air. The low proton transport number is likely due to the presence of not only oxygen vacancies but also electron holes in the bulk. This consideration is supported by the dependence of the total conductivity of $Sn_{0.9}In_{0.1}P_2O_7$ on P_{O_2}. The conductivity at 250°C was almost independent of P_{O_2} from 10^{-22} to 10^{-3} atm, while it increased gradually with increasing P_{O_2} from 10^{-3} to 1 atm.

$Sn_{0.9}In_{0.1}P_2O_7$ nominally does not contain protons in the bulk. We attempted to clarify the presence of protons in $Sn_{0.9}In_{0.1}P_2O_7$ by FTIR measurements. The infrared (IR) spectrum for $Sn_{0.9}In_{0.1}P_2O_7$ is shown in Fig. 4; the IR spectrum for SnP_2O_7 is also shown for comparison. In both IR spectra, some absorption bands appeared from 1560 to 3720 cm^{-1}, with large differences in the absorbance between the two materials. The wide absorption bands centered at 1655 and 3410 cm^{-1} are evidence of υ(OH) and δ(OH), respectively, although we cannot perfectly assign all the bands to specific vibration modes. The absorbance ratios of $Sn_{0.9}In_{0.1}P_2O_7$ to SnP_2O_7 were 5.2 and 5.7 for υ(OH) and δ(OH), respectively, which are comparable to their conductivity ratio of 4.6 at 50°C (Fig. 2). While care should be taken for water adsorbed on the sample surface, these results at least suggest that the absorption bands are mainly attributable to protons incorporated in the bulk. These results also suggest that the protons interact with the lattice oxide ions to form hydrogen bonds.

A more quantitative measurement of the proton concentration in $Sn_{0.9}In_{0.1}P_2O_7$ and SnP_2O_7 was performed using TPD of hydrogen species, and the TPD spectra are shown in Fig. 5. Water vapor and a small amount of H_2 were evolved from 260 to 1050°C. The evolution of water vapor from water adsorbed on the surface of the samples cannot be neglected, especially for data at relatively low temperatures. However, we determined the proton concentrations in $Sn_{0.9}In_{0.1}P_2O_7$ and SnP_2O_7 by assuming that all the evolved water vapor and H_2 are attributable to incorporated protons. The resulting proton concentration values were 10.4 and 2.5 mol % for $Sn_{0.9}In_{0.1}P_2O_7$ and SnP_2O_7, respectively. Note that the former value is in good agreement with the proton concentration predicted from the In^{3+} content of 10 mol %. It thus appears that the protons were fully introduced as point defects obtained by the substitution of In^{3+} for Sn^{4+}. Protons are said to dissolve in perovskite oxides such as $SrCe_{0.95}Yb_{0.05}O_{3-\alpha}$ according to Eq. 4 and 5[17]

$$H_2O(g) + V\ddot{o} \rightarrow 2H_i^{\cdot} + Oo^{x} \quad [4]$$

$$H_2O(g) + h^{\cdot} \rightarrow 2H_i^{\cdot} + \frac{1}{2}O_2(g) \quad [5]$$

Here, $V\ddot{o}$, $H_i^{\cdot}$, $h^{\cdot}$, and Oo^{x} denote an oxygen vacancy, a proton, an electron hole, and a lattice oxide ion, respectively. At present, we cannot determine whether Eq. 4 or 5 is a more predominant equilibrium for $Sn_{0.9}In_{0.1}P_2O_7$. However, Eq. 5 may be a more appropriate equilibrium for undoped SnP_2O_7 than Eq. 4, because this material has electron holes rather than oxygen vacancies as point defects. Further investigations need to be conducted to show the proton incorporation mechanism in more detail.

The H/D isotope effect on proton conductivity provides useful information on proton conduction from a different point of view. As can be seen in Fig. 6, $Sn_{0.9}In_{0.1}P_2O_7$ yielded a 1.06-1.32 times higher conductivity and a lower activation energy of 0.03 eV for a H_2O- than for a D_2O-containing atmosphere. According to the nonclassical[18] or semiclassical H/D isotope effect,[19] when the dissociation of the O–H bond is a rate-determining step for proton conduction, the activation energy for D^+ is higher than that for H^+ by a difference in zero-point energy of 0.05 eV, which is close to the difference in activation energy shown above. It is thus proposed that protons migrate via dissociation of hydrogen bonds with oxide ions in the P_2O_7 units. As described earlier, the protons migrated in $Sn_{0.9}In_{0.1}P_2O_7$ in a different way with respect to the Grotthuss mechanism.[1] Thus, a hopping mechanism is the proper interpretation of proton conduction in the present study.

An additional objective of this study was to investigate fuel-cell performance at intermediate temperatures. Fuel cell tests were conducted using $Sn_{0.9}In_{0.1}P_2O_7$ as the electrolyte at 250°C under unhumidified conditions (Fig. 7a). The EMF was about 920 mV for an electrolyte thickness of 1.2 mm, lower than the theoretical value of ~1.1 V. At least two factors are responsible for the lower EMF: (*i*)

Downloaded on 2013-08-25 to IP 133.6.32.9 address. Redistribution subject to ECS license or copyright; see ecsdl.org/site/terms_use

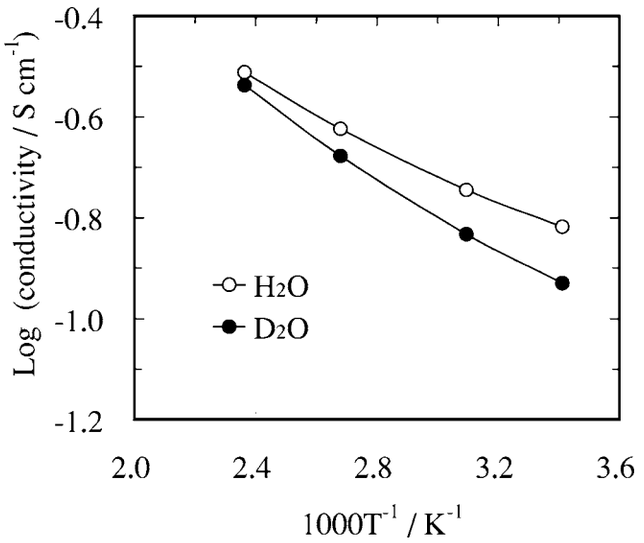

Figure 6. Isotope effect on conductivity of $Sn_{0.9}In_{0.1}P_2O_7$. The data were obtained in argon saturated with H_2O or D_2O vapor at 20°C.

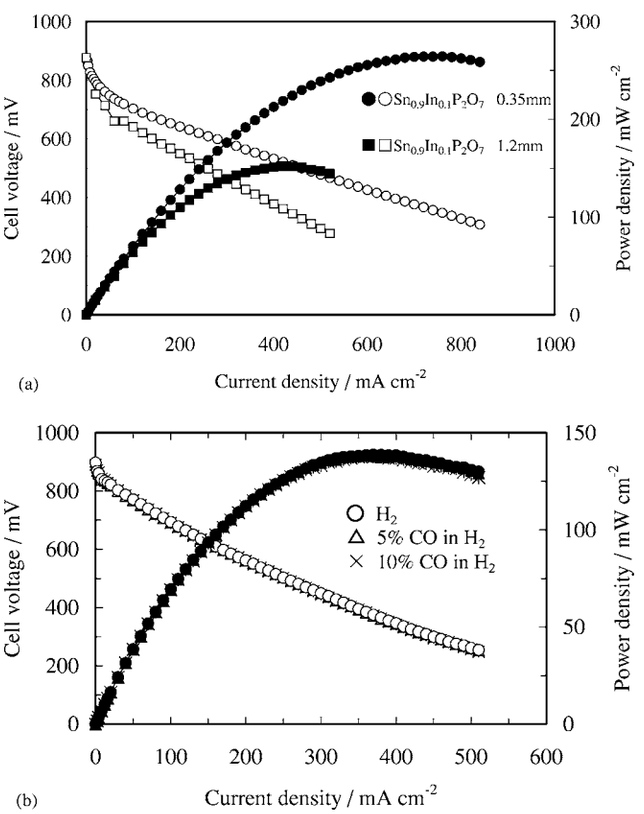

Figure 7. Fuel cell performance using $Sn_{0.9}In_{0.1}P_2O_7$ as an electrolyte. (a) Cell voltage and power density vs current density of the fuel cells using electrolyte membranes with different thicknesses at 250°C. Unhumidified hydrogen and air were supplied to the anode and cathode, respectively, at a flow rate of 30 mL min^{-1}. (b) Cell voltage and power density vs current density of the fuel cell using H_2 and a mixture of 5 or 10% CO + H_2 as fuel gases at 250°C. The electrolyte thickness was 1.2 mm. The flow rate of the fuel gases and air was 30 mL min^{-1}.

physical leakage of gas through the electrolyte since the EMF increased with increasing electrolyte thickness, and (*ii*) partial electron-hole conduction in the electrolyte causing an internal short circuit. Nonetheless, the peak power density reached 152 mW cm^{-2} with the 1.2-mm thick electrolyte. More importantly, the power density value was enhanced to 264 mW cm^{-2} by reducing the electrolyte thickness to 0.35 mm, suggesting that a thinner electrolyte can further improve fuel cell performance. However, using a current interruption method, the potential drop of the fuel cell was attributable not only to the ohmic loss but also to the cathodic polarization loss. Accordingly, another key technology for improved fuel cell performance is the development of a more active cathode.

CO tolerance tests were also conducted by supplying hydrogen or a mixture of 5 or 10% CO and hydrogen to the anode chamber at 250°C (Fig. 7b). The fuel cell performance was clearly not influenced by the presence of CO. Similar results were observed for the ac impedance spectra (0.2 V bias voltage), which maintained a polarization resistance of 0.4 Ω cm^2 regardless of the presence of CO. It was also found that the polarization resistance at 100 and 200°C in the presence of 10% CO were about 25 and 1.8 times larger, respectively, than the values at the same temperatures in pure hydrogen. This temperature dependence on CO poisoning is roughly in agreement with theoretical studies on CO tolerance at high temperatures.[20] These results indicate that the present fuel cell has excellent CO tolerance for external reformer-based applications, wherein the CO concentration in the outlet gases from conventional reformers is usually 10%.[21]

The intermediate-temperature fuel cell with the In^{3+}-doped SnP_2O_7 electrolyte exhibited a more stable performance at low relative humidities and at high CO concentrations than the PEFCs.[20] This suggests that the present fuel cell would eliminate the need for using a CO removal unit (water-gas-shift and CO preferential oxidation reactors) or a large-sized humidifier. However, several hurdles remain before the present fuel cell can be used in actual applications. In particular, cold-pressed powder pellets of In^{3+}-doped SnP_2O_7 cannot be expected to show high mechanical strength. Fabricating composites using the electrolyte and a polymer (such as polyimide or polybenzoimidazole) appears to be a promising method for improving the mechanical properties of the electrolyte membrane. This would yield flexible and durable electrolyte membranes, and facilitate the preparation of a thinner electrolyte film.

In a paper that appeared after submission of this paper, we reported that an electrochemical reactor using $Sn_{0.9}In_{0.1}P_2O_7$ as the electrolyte could reduce NOx to N_2 in the presence of excess O_2.[22]

Nagoya University assisted in meeting the publication costs of this article.

References

1. T. Norby, *Nature (London)*, **410**, 877 (2001).
2. S. M. Haile, D. A. Boysen, C. R. I. Chisholm, and R. B. Merle, *Nature (London)*, **410**, 910 (2001).
3. T. Kenjo and Y. Ogawa, *Solid State Ionics*, **76**, 29 (1995).
4. T. Matsui, S. Takeshita, Y. Iriyama, T. Abe, M. Inaba, and Z. Ogumi, *Electrochem. Commun.*, **6**, 180 (2004).
5. D. A. Boysen, T. Uda, C. R. I. Chisholm, and S. M. Haile, *Science*, **303**, 68 (2004).
6. W. Wieczorek, G. Zukowska, R. Borkowska, S. H. Chung, and S. Greenbaum, *Electrochim. Acta*, **46**, 1427 (2001).
7. A. Matsuda, T. Kanzaki, K. Tadanaga, M. Tatsumisago, and T. Minami, *Solid State Ionics*, **154–155**, 687 (2002).
8. J. D. Kim and I. Honma, *Electrochim. Acta*, **49**, 3179 (2004).
9. C. Yang, S. Srinivasan, A. B. Bocarsly, S. Tulyani, and J. B. Benziger, *J. Membr. Sci.*, **237**, 145 (2004).
10. A. Takeuchi, M. Nagao, P. Heo, M. Sano, T. Hibino, and A. Tomita, in *Proceedings of Presentation at the 72th Meeting of The Electrochemical Society of Japan*, Kumamoto, April 1–3, 2005, p. 197 (2005).
11. P. K. Gover, N. D. Withers, S. Allen, R. L. Withers, and S. O. Evans, *J. Solid State Chem.*, **166**, 42 (2002).
12. S. Gallini, M. Hänsel, T. Norby, M. T. Colomer, and J. R. Jurado, *Solid State*

Downloaded on 2013-08-25 to IP 133.6.32.9 address. Redistribution subject to ECS license or copyright; see ecsdl.org/site/terms_use

Ionics, **162–163**, 167 (2003).
13. K. Amezawa, Y. Tomii, and N. Yamamoto, *Solid State Ionics*, **162–163**, 175 (2003).
14. H. Iwahara, T. Yajima, T. Hibino, and H. Ushida, *J. Electrochem. Soc.*, **140**, 1687 (1993).
15. S. Steinsvik, Y. Larring, and T. Norby, *Solid State Ionics*, **143**, 103 (2001).
16. N. Bonanos, *Solid State Ionics*, **145**, 265 (2001).
17. H. Uchida, N. Maeda, and H. Iwahara, *Solid State Ionics*, **11**, 117 (1983).
18. T. Norby, *Solid State Ionics*, **40–41**, 857 (1990).
19. A. S. Nowick and A. V. Vaysleyb, *Solid State Ionics*, **97**, 17 (1997).
20. C. Yang, P. Costamagna, S. Srinivasan, J. Benziger, and A. B. Bocarsly, *J. Power Sources*, **103**, 1 (2001).
21. M. Levent, D. J. Gunn, and M. A. El-Bousiffi, *Int. J. Hydrogen Energy*, **28**, 945 (2003).
22. M. Nagao, T. Yoshii, T. Hibino, M. Sano, and A. Tomita, *Electrochem. Solid-State Lett.*, **9**, J1 (2005).

Downloaded on 2013-08-25 to IP 133.6.32.9 address. Redistribution subject to ECS license or copyright; see ecsdl.org/site/terms_use